Lab on a Chip

Accepted Manuscript

This is an *Accepted Manuscript*, which has been through the Royal Society of Chemistry peer review process and has been accepted for publication.

Accepted Manuscripts are published online shortly after acceptance, before technical editing, formatting and proof reading. Using this free service, authors can make their results available to the community, in citable form, before we publish the edited article. We will replace this *Accepted Manuscript* with the edited and formatted *Advance Article* as soon as it is available.

You can find more information about *Accepted Manuscripts* in the Information for Authors.

Please note that technical editing may introduce minor changes to the text and/or graphics, which may alter content. The journal's standard Terms & Conditions and the Ethical guidelines still apply. In no event shall the Royal Society of Chemistry be held responsible for any errors or omissions in this *Accepted Manuscript* or any consequences arising from the use of any information it contains.

ROYAL SOCIETY OF CHEMISTRY

www.rsc.org/loc

Please do not adjust margins

Lab on a Chip

ARTICLE

Geometric Effects in Microfluidics on Heterogeneous Cell Stress using an Eulerian-Lagrangian Approach

Received 00th January 20xx,
Accepted 00th January 20xx

DOI: 10.1039/x0xx00000x

www.rsc.org/

K. M. Warren[a], J. N. Mpagazehe[a], P. R. LeDuc[a,b+], and C. F. Higgs III[a] *

The response of individual cells at the micro-scale in cell mechanics is important in understanding how they are affected by changing environments. To control cell stresses, microfluidics can be implemented since there is tremendous control over the geometry of the devices. Designing microfluidic devices to induce and manipulate stress levels on biological cells can be aided by computational modeling approaches. Such approaches serve as an efficient precursor to fabricating various microfluidic geometries that induce predictable levels of stress on biological cells, based on their mechanical properties. Here, a three-dimensional, multiphase computational fluid dynamics (CFD) modeling approach was implemented for soft biological materials. The computational model incorporates the physics of the particle dynamics, fluid dynamics and solid mechanics, which allows us to study how stresses affect the cells. By using a Eulerian-Lagrangian approach to treat the fluid domain as a continuum in the microfluidics, we are conducting studies of the cells' movement and the stresses applied to the cell. As a result of our studies, we were able to determine that a channel with periodically alternating columns of obstacles was capable of stressing cells at the highest rate, and that microfluidic systems can be engineered to impose heterogenous cell stresses through geometric configuring. We found that when using controlled geometries of the microfluidics channels with staggered obstructions, we could increase the maximum cell stress by nearly 200 times over cells flowing through microfluidic channels with no obstructions. Incorporating computational modeling in the design of microfluidic configurations for controllable cell stressing could help in the design of microfludic deviecs for stressing cells such as cell homogenizers.

1. Introduction

Microfluidics has been used in a variety of lab-on-a-chip applications to study the response of cells to different stimuli including chemical, electrical, and mechanical inputs [1-4]. Variations in the fluid flow in microfluidic systems affect the behaviour of cells within the fluid domain and applications in this area include cell cultivation, adhesion, lysis, and stressing [5-8]. Mechanically stimulating cells can result in an array of cell signalling responses including those for proliferation, differentiation, and apoptosis [9-13]. Here we focus on examining the fluid stress applied to individual cells in microfluidic systems with controlled geometries. To understand this, we developed a computational fluid dynamics (CFD) approach to determine microfluidic flows and configurations that will increase stresses experienced by individual cells. We were able to computationally evaluate how stresses affect individual cells and correlate their heterogeneous response to the differences in geometric microfluidic configuration. This approach will help develop a greater understanding of the mechanical response of individual cells from fluid stresses in microfluidics, but also can play an important role in future technologies such as in protein extraction and cell lysis in areas such as pharmaceuticals and biofuels.

2 Microfluidic Computational Modelling Framework

Modelling stress on cells in fluid flow is important in many areas such as haematology. Although models have been developed, the ability to use multiphase approaches that allow for combined solid domains to be dictated by viscous flows while enabling the cell to be tracked throughout the fluid domain **[14, 15]** have not been readily available and transparent. This type of model would provide a robust approach for understanding cell stresses in microfluidic systems. To accomplish this, one assumes the particles follow the fluid velocity streamlines **[16]** or that cells act as the fluid in the system, and thus are accounted for in the fluid domain for computational modelling **[17]**. Our approach focuses on the computational incorporation of cells within fluid flow to increase the amount of stress applied to cells through geometric changes using an Eulerian-Lagrangian approach. With an Eulerian approach, the primary media, the fluid, is treated as a continuum. Alternatively, in a Lagrangian approach, the secondary media, the biological cells, are treated as discrete particles.

In our approach, the fluid domain is treated with an Eulerian approach and the cells with a Lagrangian approach. We first modified the existing Eulerian-Lagrangian approach to account for the fluid

[a] Department of Mechanical Engineering, Carnegie Mellon University, 5000 Forbes Ave, Pittsburgh, Pennsylvania, 15213, USA
[b] Departments of Biomedical Engineering, Computational Biology, and Biological Sciences,
+Carnegie Mellon University, 5000 Forbes Ave, Pittsburgh, Pennsylvania, 15213, USA E-mail: prl@andrew.cmu.edu; Fax: +1 412-268-3348; Tel: +1 412-268-2504
[c] *Carnegie Mellon University, 5000 Forbes Ave, Pittsburgh, Pennsylvania, 15213, USA E-mail: higgs@andrew.cmu.edu; Fax: +1 412-268-3348; Tel: +1 412-268-2486

This journal is © The Royal Society of Chemistry 2015

Lab on a Chip Accepted Manuscript

Please do not adjust margins

stress acting on the individual cells, and then we vary the overall microfluidic geometries to assess their impact on stress levels; a fibroblast was used as a model cell here. Figure 1 shows a microfluidic device with cell stresses under a controlled geometry.

2.1 Modelling the fluid domain using the Eulerian approach

The software used in this study was the custom Particle-Surface Tribology Analysis Code (P-STAC), a computational tool developed to create multiphysics CFD simulations of multiphase (fluid-particle) systems [18-21]. To model the fluid phase in the domain, the Navier-Stokes momentum equations, Eq. 1-4, were approximated using the Chorin projection method [9, 22, 23]. In the Navier Stokes equation, g is the gravitational acceleration, t is time, ρ is density, μ is the fluid viscosity, u, v, and w are the fluid velocities in the x, y, and z directions, respectively. In the momentum equations, Eq. 1-3, velocity components are solved using an Euler time-stepping algorithm. In the continuity equation (Eq. 4), pressure is solved using successive over-relaxation (SOR) and the pressure and velocity are coupled together.

$$\rho\left(\frac{\partial u}{\partial t}+u\frac{\partial u}{\partial x}+v\frac{\partial u}{\partial y}+w\frac{\partial u}{\partial z}\right)=-\frac{\partial p}{\partial x}+\mu\left(\frac{\partial^2 u}{\partial x^2}+\frac{\partial^2 u}{\partial y^2}+\frac{\partial^2 u}{\partial z^2}\right)+\rho g_x \quad (1)$$

$$\rho\left(\frac{\partial v}{\partial t}+u\frac{\partial v}{\partial x}+v\frac{\partial v}{\partial y}+w\frac{\partial v}{\partial z}\right)=-\frac{\partial p}{\partial y}+\mu\left(\frac{\partial^2 v}{\partial x^2}+\frac{\partial^2 v}{\partial y^2}+\frac{\partial^2 v}{\partial z^2}\right)+\rho g_y \quad (2)$$

$$\rho\left(\frac{\partial w}{\partial t}+u\frac{\partial w}{\partial x}+v\frac{\partial w}{\partial y}+w\frac{\partial w}{\partial z}\right)=-\frac{\partial p}{\partial z}+\mu\left(\frac{\partial^2 w}{\partial x^2}+\frac{\partial^2 w}{\partial y^2}+\frac{\partial^2 w}{\partial z^2}\right)+\rho g_z \quad (3)$$

$$\frac{\partial u}{\partial x}+\frac{\partial v}{\partial y}+\frac{\partial w}{\partial z}=0 \quad (4)$$

The fluid domain is discretised using a finite-difference method. Rectangular mesh geometries that were smaller than the particle size were chosen for the fluid domain (Fig. 1a). The boundary conditions consist of no-slip on the top and bottom walls (y-direction), forward and backward walls (z-direction); velocity inlet on the left wall (x-direction); and a pressure outlet on the right wall (x-direction). All simulations have an inlet velocity of 10mm/s and maintain a Reynolds number less than 1 with consistent fluid and cell properties (Table 1) with microfluidic dimensions of 100 µm x 25 µm x 25 µm. The right wall's pressure was set to 0 Pa resulting in a pressure distribution across the length of the microfluidic system (Fig. 1b). The velocity streamlines (Fig. 1c) and cell stresses (Fig. 1d) reveal heterogeneous responses through our microfluidic systems.

Table 1 Properties of the Cells, Fluid, and Channel Walls

Cell Properties					Fluid Properties		Channel Walls
Radius	Solid Fraction	Mass	Density	Elastic Modulus	Density	Viscosity	Spring Coefficient
4.22 µm	5%	27×10^{-12} g	0.0011 g/mm^3	7500 Pa [6]	9.8 kg/mm^3	0.4 mPa·s	100 N/mm

2.2 Modelling cells using a Lagrangian approach

The cells are modelled as spheres within this framework based on their tendency to become spherical when not attached to a substrate [24]. The Lagrangian phase of the microfluidic channel consists of only the cells and the discrete element method was used to computationally model collisions between cells and the walls of the channel using a spring-dashpot model (Eq. 5) where F is the force applied to the cell, K_{spring} is the spring constant of the cell, d is the spring compression distance, V_n is the relative normal velocity of the colliding cells, and $B_{dashpot}$ is the damping coefficient. The spring constant was calculated using Equation 6 based on the assumption of Hertzian contact where only small deflections (d = 10%) are experienced. Here, E^* represents the Young's Modulus (or elastic modulus) and R' is the reduced radius.

$$\vec{F}=K_{spring}\times\vec{d}-\vec{V_n}\times B_{dashpot} \quad (5)$$

$$K_{spring}=\frac{4E^*}{3\sqrt{R'}}\times d^{3/2} \quad (6)$$

$$\frac{1}{E^*}=\frac{1-v_1^2}{E_1}+\frac{1-v_2^2}{E_2} \quad (7)$$

$$\frac{1}{R'}=\frac{1}{R_1}+\frac{1}{R_2} \quad (8)$$

$$B_{dashpot}=\sqrt{\frac{K_{spring}}{mass}} \quad (9)$$

$$dT=C\sqrt{(mass/K_{spring})} \quad (10)$$

The P-STAC framework checks for collisions at each time step, which is set before the initiation of the simulation. To determine the time step (dT), a general spring-mass system is used as shown in Equation 10 where the constant C is 0.2 [25].

2.3 Coupling fluid and solid domains using Stokes approach

Calculating each cell's stresses uses the coupling of the fluid and solid domains through a Stokes assumption. The Stokes assumption is used for domains where the flow is laminar, which is the case in our microfluidics approach. The Stokes drag force (Eq. 11) represents the effect of the fluid on the fibroblasts and is calculated for x, y, and z directions. Here μ is viscosity, r is the radius of the cell, and v is the cell velocity in relation to the fluid velocity. The cell's new position is calculated from the Stokes drag and using Newton's 2nd law [18].

$$F_{Stokes\ Drag}=6\pi\mu r v \quad (11)$$

In the calculation of the stress on the biological cells, the comparative stress theory allows us to utilize the fluid viscous stresses and apply them to the cells using von Mises yield criterion, which results in the overall stress as shown in Equation 14 [22, 26]. Here, the viscous stresses and the normal stresses are maximized. In these equations p is pressure, λ is a thermodynamic material constant of viscosity, τ is the viscous part of the stress tensor σ, and δ is the strain tensor. This stress is applied to the cells resulting in stress on individual cells (Fig. 1d).

The current model predicts the stress experienced by cells in microfluidic channels, although the model does not have two way particle-fluid coupling. As a result, the fluid affects the cells but the cells do not affect the fluid in this model. However, this model provides insight for understanding how the physics-based movement

Lab on a Chip Accepted Manuscript

This journal is © The Royal Society of Chemistry 2015

of cells to different locations of the microfluidic channel can affect the stress that the cells experience.

$$\boldsymbol{\sigma} := -p\boldsymbol{I} + \boldsymbol{\tau} := (-\boldsymbol{p} + \boldsymbol{\lambda} div\vec{\boldsymbol{u}})\boldsymbol{I} + 2\boldsymbol{\mu}\boldsymbol{\delta} \quad (12)$$

$$\boldsymbol{\delta} := \frac{1}{2}\left[\left(\frac{\partial u_i}{\partial x_j} + \frac{\partial u_j}{\partial x_i}\right)\right]_{i,j=1,2,3} \quad (13)$$

$$\sigma_{scalar} = \left[\frac{1}{6}\sum(\sigma_{ii} - \sigma_{jj})^2 + \sum \sigma_{ij}^2\right]^{\frac{1}{2}} \quad (14)$$

3 Results and Discussion

To study how cells are stressed when altering the geometric environment of the microfluidics, controlled configurations were implemented and evaluated using P-STAC. The fluid field was allowed to reach quasi-steady state before the particle dynamics of the cells were simulated. Additionally, the CFD solver was suspended once steady state was reached in order to decrease computational time. Figure 2 shows how the von Mises stresses on the cells altered over time as the cells individually pass through the constricted channel geometry. The von Mises stress levels (whose magnitude in *Pa*) is indicated by the color of the cells themselves. A snapshot was taken at designated times to compare the maximum amount of stress experienced by the cells within that time domain. As the cells approach areas of constriction, their stress levels increase. This is attributed to the fluid velocity (whose magnitude in *mm/s* is indicated by channel color) increasing relative to the cell's velocity, which induces high shear stress on the cells.

The stress on each cell was directly correlated to the geometry in the microfluidic system. To investigate this, we designed configurations of the microfluidics and computationally analysed the cell stresses that resulted (Fig. 3). As each grey obstruction block is 25% of the channel height, geometries in 3c, 3d, and 3e have flow that is constricted by 50%.

The stresses of each of the cells are shown in the histogram plots for each respective geometry (Fig. 3-right side panels). Each cell is individually tracked as labelled in Figure 3 and maintain the same identifying number in each histogram. These cells were started at the same point of each simulation. The two cells that are at the end of the channel were not accounted for in these plots and are discarded to the right of the channel because the time step utilized was too large for the discrete element modelling to capture their movement. By doing this, we were able to decrease the computational time while accurately simulating the other particles in the flow [22].

From the computational model, there is the least amount of stress on the cells when there is no obstruction present. Although the obstruction free microfluidic design has a high fluid velocity of 16.5 mm/s throughout most of the channel, the cells' velocities are near that of the fluid as discussed previously (equation 11). All of the obstruction-containing geometries allowed for the majority of the cells to be stressed above 80% of the maximum stress experienced within the simulation. This is important when a configuration with the maximum amount of cells stressed is desired.

The periodically alternating columns of obstacles configuration (shown in Fig 3e) produced the greatest amount of stress on the cells with greater than 175 times increase over the no obstruction case (Fig. 4). This seems to be due to both the constriction size and the repeated offset locations of the obstructions in the flow. Additionally, adding an offset row of these spaced obstructions increases the stress values.

Along with studying the obstructions' effects on stress within a microfluidic channel, we examined how other parameters would affect the amount of stress on the cells. The concentration of the cells within the media, fluid velocity, fluid density, and fluid viscosity were varied (Fig. 5). The velocity and viscosity are the only parameters that seem to dramatically affect the cell's stress level. Because of the no-slip boundary conditions (i.e., the fluid velocity at the walls is zero), there are greater velocity gradients within the channel as the input velocity increases, and the stresses on the cells will increase as either the velocity gradients increase or the fluid viscosity. While increases in the concentration of cells has a moderately proportional impact on the cell stress, the changes in fluid density seems to affect all the viscous stresses the same so that there is no net change.

4 Conclusions

To investigate the stress effects on cells by changing the geometrical configurations of a microfluidic channel, an in-house computational tool, which includes fluid dynamics, particle dynamics, and solid mechanics, was modified to incorporate a modified von Mises stress. The modified von Mises stress enables one to quantify and track the effect of the surrounding fluid flow field on each moving cells. After testing various geometries, the flow configuration that produced the most amount of stress on the cells was the periodically alternating columns of obstacles geometry, which showed a tremendous increase in the maximum stress. Having multiple obstructions even of the same configuration also increased the stress. This work is advantageous because we can begin to characterize effects of stress on cell-like material in microfluidic environments while virtually testing the system before conducting expensive and time-consuming experimentation. In addition to studying the resulting stress on the cell, we can change the fluid environment and type of cells within the computational domain to optimize experiments within the laboratory. The results of these findings will be of great interest to researchers and industry working in lab-on-a-chip, cell mechanics, and fluid flow arenas.

Acknowledgements

This work was supported by the Gates Millennium Scholarship Program and an Alfred P. Sloan Foundation Fellowship. This work was supported in part also by the National Science Foundation (CMMI-1100430, CMMI-1160840, CPS-1135850, CMMI-0645124), and the Air Force Office of Scientific Research (FA9550-13-1-01 08).

Lab on a Chip Accepted Manuscript

Please do not adjust margins

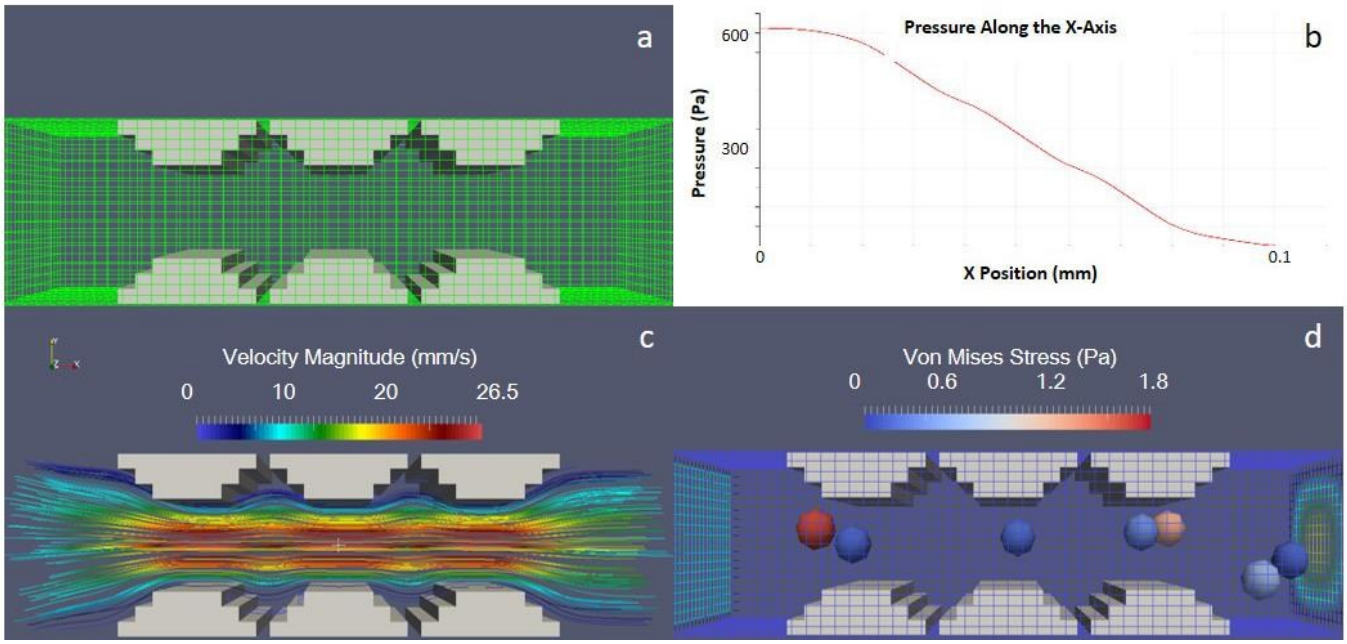

Fig. 1 Geometrically-controlled microfluidics for inducing heterogeneous cell stress through an Eulerian-Lagrangian approach. a) The mesh for the microfluidic channel is used to calculate pressure at the center of each fluid cell (mesh cube). The velocities, u, v, and w, are calculated on the perimeter of each mesh cell. b) Pressure drop along the length of the channel. c) The velocity streamlines for this microfluidic configuration. d) The stress on each particle, or fibroblast cell, is calculated based on Equation 10c. The dimensions of this microfluidic channel are 100um x 25 um x 25um

Lab on a Chip Accepted Manuscript

This journal is © The Royal Society of Chemistry 2015

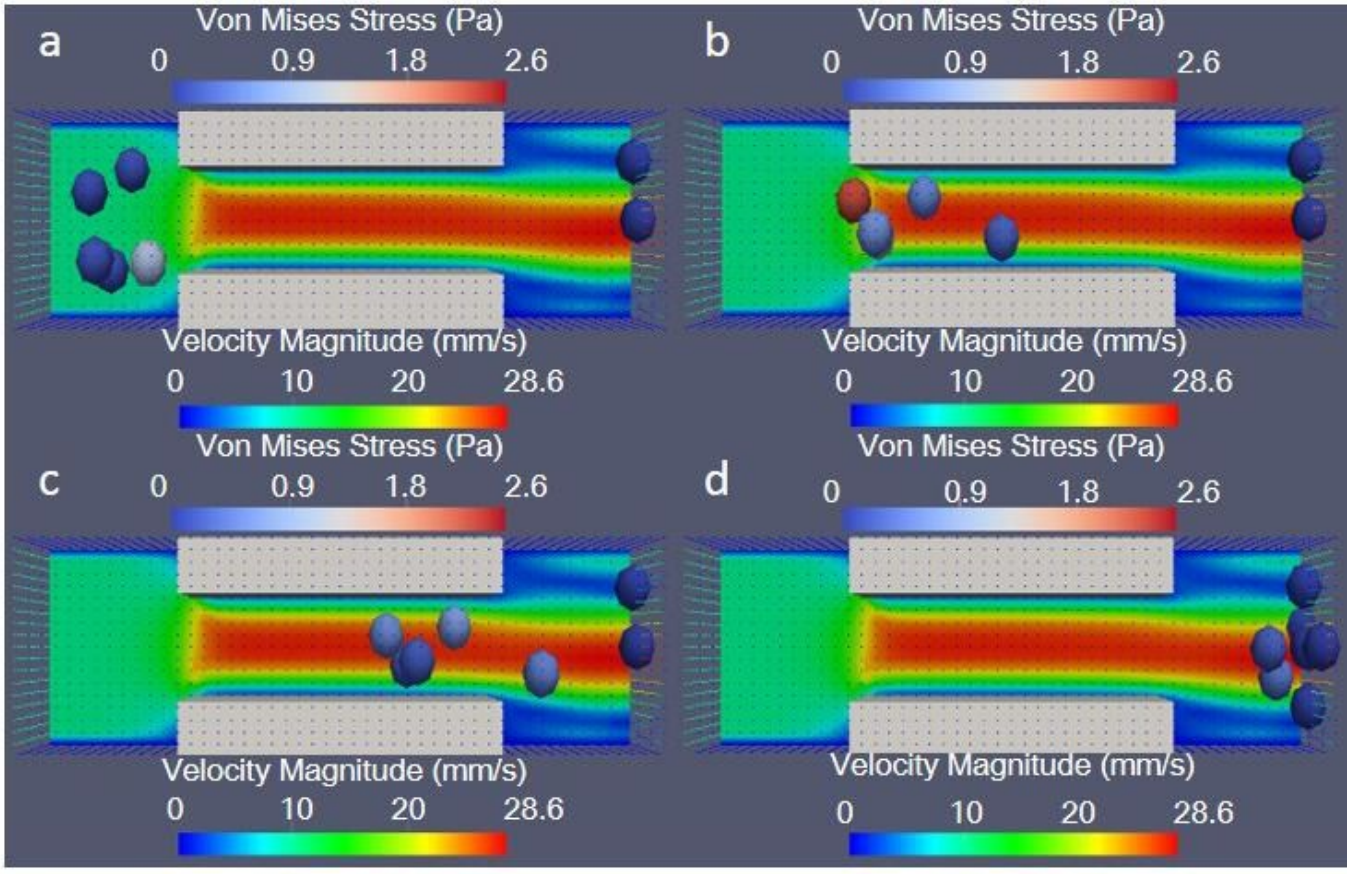

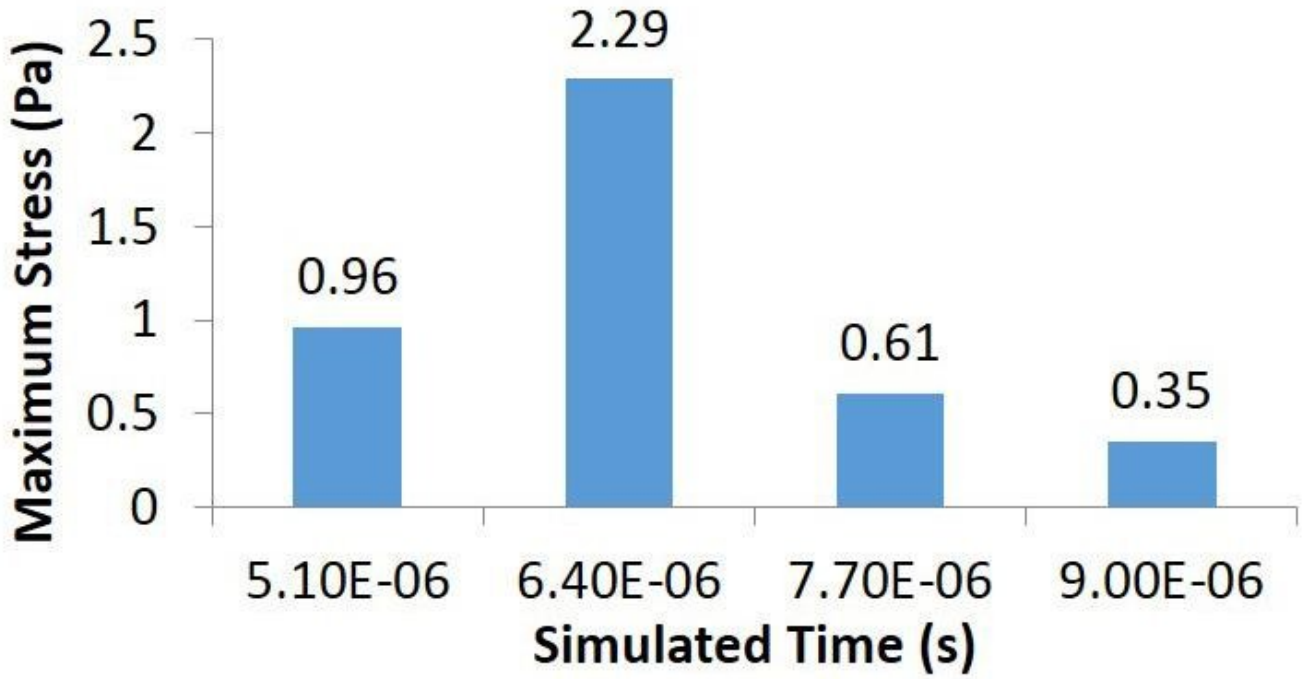

Fig. 2 The stresses on the cells as they move through the channel geometry. Cells moving through microfluidic channels with a controlled geometry due to a constriction (grey) have different stresses at each time point: a) t=5.1 $\times 10^{-6}$ s, b) t=6.4 $\times 10^{-6}$ s, c) t=7.71$\times 10^{-6}$ s, and d) t=9.0 $\times 10^{-6}$ s. e) The maximum stress experienced at a given time for the cells.

Lab on a Chip Accepted Manuscript

Please do not adjust margins

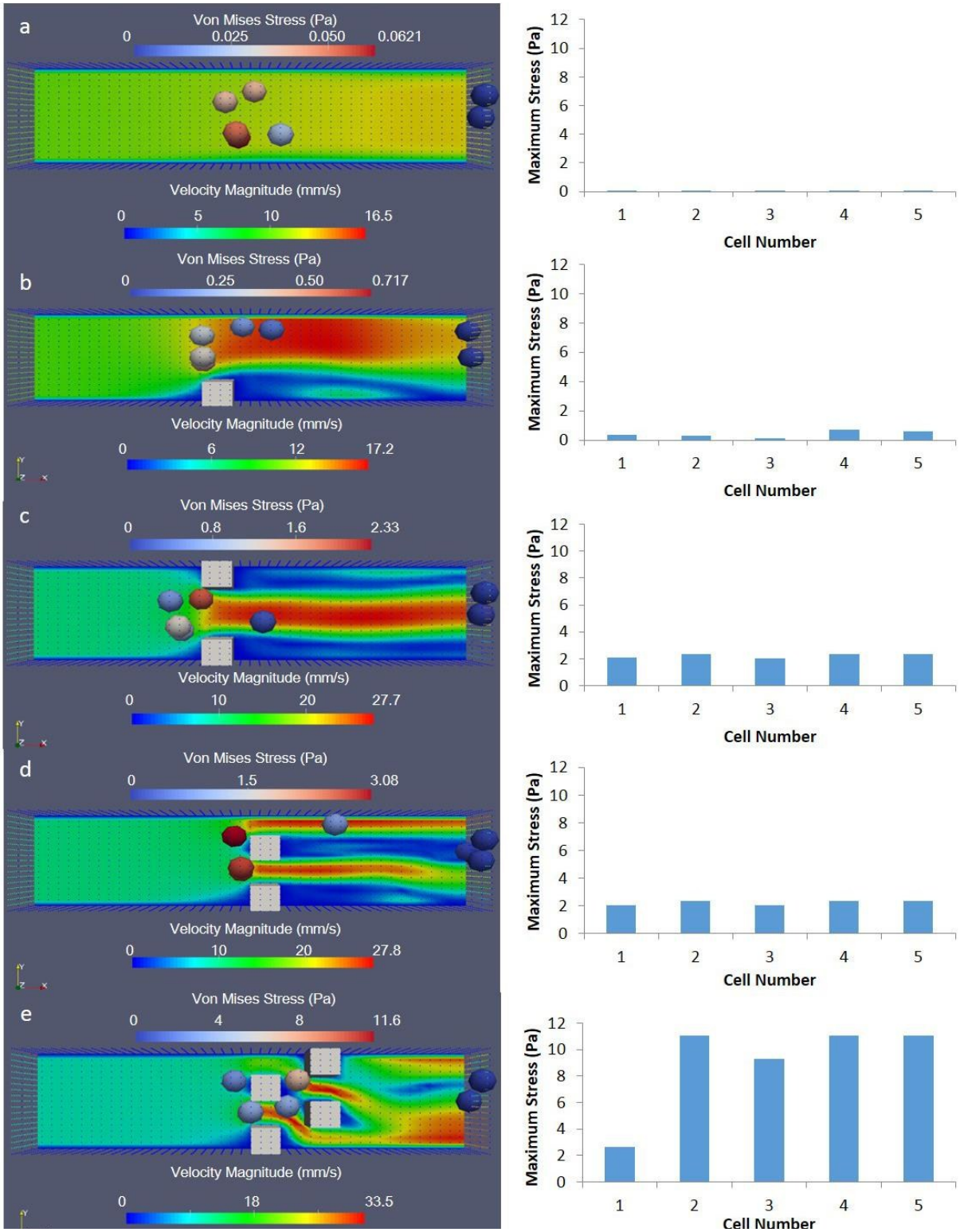

Fig. 3 Controlled geometries for our microfluidic systems were designed and evaluated to understand cell stress response. The geometries included a) No obstruction, b) Single square obstructions blocking 25% of the channel width, c) Mirror square obstructions on opposite walls blocking 50% of the channel width, d) Mirror square obstructions spaced across the channel width blocking 50% of the width, and e) periodically alternating columns of obstacles spaced across the channel width blocking 50% of the channel width. Each geometry's respective histogram (right side panels on figure) displays the maximum stress experienced throughout the simulation for each cell.

Lab on a Chip Accepted Manuscript

This journal is © The Royal Society of Chemistry 2015

Fig. 4 The maximum stress experienced by cells in each microfluidic configuration studied.

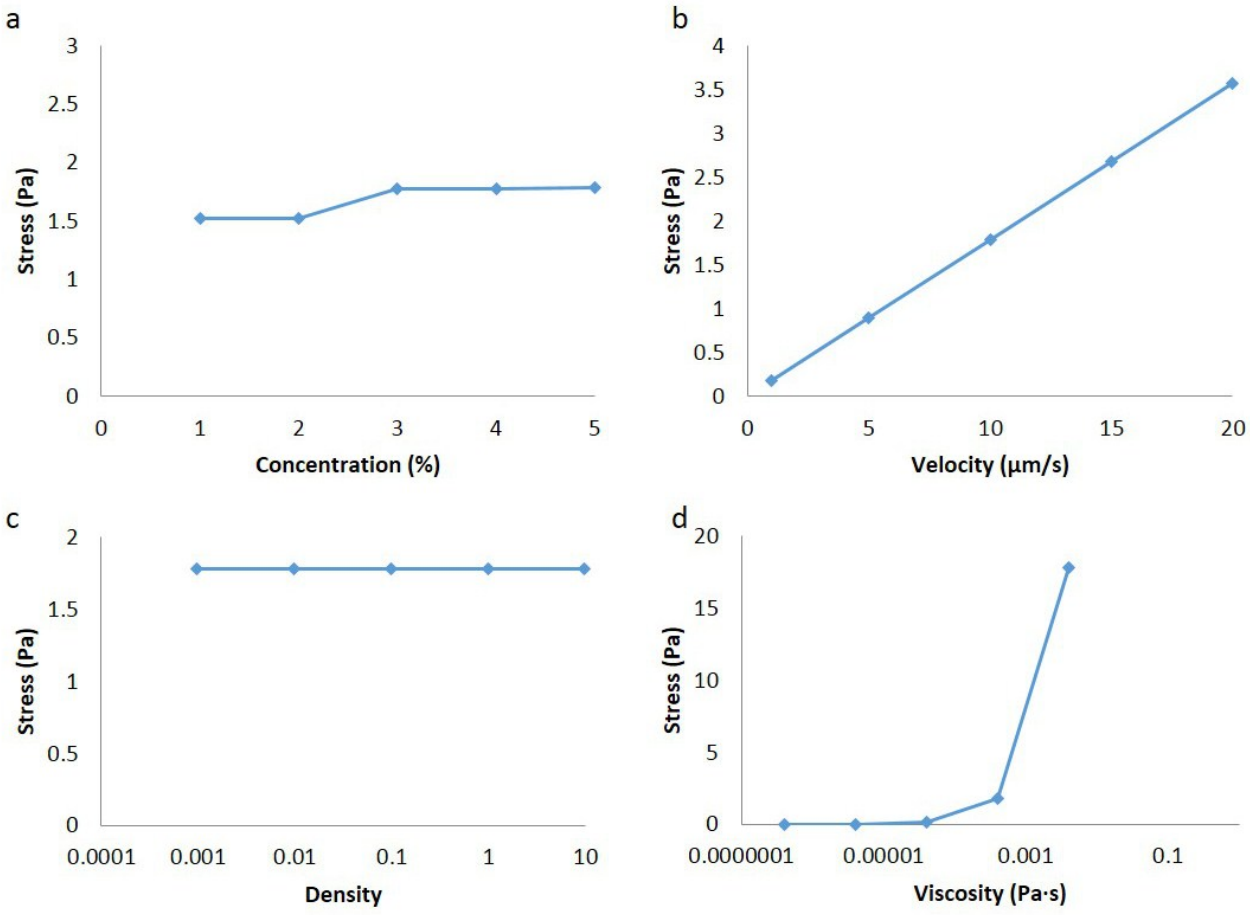

Fig. 5 Results of a parametric study of various parameters on cell stress. The effects of a) Cell concentration, b) Fluid velocity, c) Fluid density, and d) Fluid viscosity were examined.

Lab on a Chip Accepted Manuscript

Please do not adjust margins

References

1. H. A. Stone, A. D. Stroock and A. Ajdari, *Annual Review of Fluid Mechanics*, 2004, **36**, 381-411.
2. A. D. Stroock, S. K. Dertinger, A. Ajdari, I. Mezic, H. A. Stone and G. M. Whitesides, *Science*, 2002, **295**, 647-651.
3. S. M. Vuong and S. L. Anna, *Biomicrofluidics*, 2012, **6**, 22004-2200418.
4. K. M. Warren, J. N. Mpagazehe, P. R. LeDuc and C. F. Higgs, *Appl Phys Lett*, 2014, **105**, 163701.
5. H. Hufnagel, A. Huebner, C. Gulch, K. Guse, C. Abell and F. Hollfelder, *Lab Chip*, 2009, **9**, 1576-1582.
6. J. Solon, I. Levental, K. Sengupta, P. C. Georges and P. A. Janmey, *Biophys J*, 2007, **93**, 4453-4461.
7. D. Di Carlo, K. H. Jeong and L. P. Lee, *Lab Chip*, 2003, **3**, 287-291.
8. D. Huh, H. Fujioka, Y. C. Tung, N. Futai, R. Paine, 3rd, J. B. Grotberg and S. Takayama, *Proc Natl Acad Sci U S A*, 2007, **104**, 18886-18891.
9. B. E. Sumpio, A. J. Banes, L. G. Levin and G. Johnson, *Joural of Vascular Surgery*, 1987, **6**, 252-256.
10. K. Yamamoto, T. Sokabe, T. Watabe, K. Miyazono, J. K. Yamashita, S. Obi, N. Ohura, A. Matsushita, A. Kamiya and J. Ando, *Am J Physiol Heart Circ Physiol*, 2005, **288**, H1915-1924.
11. M. Mayr, Y. Hu, H. Hainaut and Q. Xu, *FASEB J*, 2002, **16**, 1423-1425.
12. J. Sadoshima and S. Izumo, *Annual Review of Physiology*, 1997, **59**, 551-571.
13. R. L. Steward, Jr., C. M. Cheng, J. D. Ye, R. M. Bellin and P. R. LeDuc, *Sci Rep*, 2011, **1**, 147.
14. M. Wurm and A. P. Zeng, *Lab Chip*, 2012, **12**, 1071-1077.
15. M. V. Kameneva, G. W. Burgreen, K. Kono, B. Repko, J. F. Antaki and M. Umezu, *ASAIO Journal*, 2004, **50**, 418-423.
16. L. Gu and W. A. Smith, *ASAIO Journal*, 2005, **51**, 202-207.
17. R. Zhao, J. F. Antaki, T. Naik, T. N. Bachman, M. V. Kameneva and Z. J. Wu, *Biorheology*, 2006, **43**, 747-765.
18. M. C. Marinack, J. N. Mpagazehe and C. F. Higgs, *Powder Technology*, 2012, **221**, 47-56.
19. J. N. Mpagazehe and C. F. Higgs, *Journal of Engineering Tribology*, 2013, **227**, 777-786.
20. J. N. Mpagazehe, A. F. Queiruga and C. F. Higgs, *Tribology International*, 2013, **59**,
21. Y. Guo, C. Y. Wu, K. D. Kafui and C. Thornton, *Powder Technology*, 2011, **206**, 177-188.
22. M. Griebel, T. Dornseifer and T. Neunhoeffer, SIAM, 1998,
23. E. J. Terrell and C. F. Higgs, *Journal of Tribology*, 2008, **131**, 1-10.
24. M. T. Armstrong and P. B. Armstrong, *Cell Motility*, 1980, **1**, 99-112.
25. C. O'Sullivan and J. D. Bray, *Engineering Computations*, 2004, **21**, 278-303.
26. C. Bludszuweit, *Artificial Organs*, 2008, **19**, 590-596.

Lab on a Chip Accepted Manuscript

This journal is © The Royal Society of Chemistry 2015